CHEMICAL ENGINEERING TRANSACTIONS
VOL. 73, 2019
A publication of AIDIC
The Italian Association of Chemical Engineering
Online at www.aidic.it/cet
Guest Editors: Andrea D'Anna, Paolo Ciambelli, Carmelo Sunseri

ISBN 978-88-95608-70-9; **ISSN** 2283-9216
DOI: 10.3303/CET1973027

CFD Model of Agitated Vessel for the Removal of Cr(VI) by Nano-Hematite Particles

Giorgio Vilardi*, Marco Stoller, Luca Di Palma, Nicola Verdone

University of Rome "La Sapienza", Dept. of Chemical Materials Environmental Eng., Via Eudossiana 18, 00184 Rome, Italy
giorgio.vilardi@uniroma1.it

The mixing operation and design of agitated vessels for various chemical engineering applications may still represent a challenge due to the complexity of hydrodynamic fields established inside the reaction system. Computational Fluid Dynamics (CFD) is considered a valuable tool for the investigation of the complex turbulent flow field proper of mechanically agitated vessel (MAV). The use of CFD may effectively support the process engineer for the selection of the most proper impeller/vessel geometry and operative conditions to achieve homogeneous and fully turbulent conditions. In this work, experimental tests and CFD simulations were performed to study the Cr(VI) removal efficiency through nano-hematite particles (nHP) in MAV. More in detail, some solutions of Cr(VI) were treated using lab-made nHP, produced by a spinning disk reactor, in lab-scale agitated vessel and the kinetic of the removal process was experimentally studied varying the reactor/impeller configuration (impeller geometry) and the impeller rotational velocity. The obtained results were interpreted according to a CFD model of the system hydrodynamic field based on the k-ε turbulent model whereas the kinetic data were fitted to a suitable mass transfer kinetic model.

1. Introduction

Wastewater treatment still represents a severe issue in Europe (Patterer et al., 2017) and various researchers have been developed nano-based technology to deals with it (Bavasso et al., 2018a). In the last decade the number of applications of nanostructured materials has growth remarkably in various fields, such as chemicals production (Konuray et al., 2017), materials improvement (Genova et al., 2017), materials modification (Stoller et al., 2018), catalysis (Di Pascasio et al., 2016) and environmental processes. Considering the latter processes, valuable studies have been published regarding the use of iron-based nanoparticles (Bavasso et al., 2018b) also for the modification of membranes used to treat highly polluted wastewaters (Bavasso et al., 2017). Hexavalent Chromium (Cr(VI)) is one of the most hazardous compounds present in the Mediterranean Area, considering its high carcinogenic potential and elevated mobility in environmental media (Acar and Malkoc, 2004). Cr(VI) is very soluble in water and tends to generate oxyanions species in a wide range of pH and concentrations, thus Cr(VI) species are mainly present as anions in aqueous environments. The use of nano-sorbent materials for the removal of heavy metals represents an important field of nanotechnology application (Stoller et al., 2017), and iron-based nano-materials have already proved to be very efficient towards the removal of heavy metals such as Cr(VI) species (Xiao et al., 2015). Most studies reported remarkable Cr(VI) sorption capacities by the use of nano-iron oxides materials, such as magnetite (149.3 mg/g at 25°C (Chen et al., 2018)), maghemite (38.57 mg/g at 25°C (Nematollahzadeh et al., 2015)) and hematite (140.4 mg/g at 20°C (Singh et al., 1993)) working in magnetically stirred tanks, using liquid volumes in the range 50-150 mL. Therefore, no data obtained using scalable equipment, such as Rushton equipped stirred tank used in the present work, have been provided in literature. The performances in sorption processes are strongly influenced by the hydrodynamic field established inside the reactor vessel, since mass transfer rate depends not only on the system geometry, chemical nature of the compounds and operative conditions (temperature, pressure etc.) but it is strongly related to the Reynolds number, i.e. to the flow regime (Scargiali et al., 2014). To this aim, the present study reports some experimental data about the kinetic of Cr(VI) sorption by lab-made nano-hematite particles in Rushton equipped agitated vessel, providing some interpretation of the

Paper Received: 30 March 2018; Revised: 16 August 2018; Accepted: 23 March 2019

Please cite this article as: Vilardi G., Stoller M., Di Palma L., Verdone N., 2019, CFD Model of Agitated Vessel for the Removal of Cr(vi) by Nano-hematite Particles , Chemical Engineering Transactions, 73, 157-162 DOI:10.3303/CET1973027

obtained modelling results, such as mass transfer coefficient, through computational fluid dynamic modelling of the established flow field in the vessel, varying the impeller rotational velocity.

2. Materials and Methods

2.1 Materials

All the reagents were purchased from Sigma Aldrich (Milan) and were of analytical grade or higher. The solutions were prepared in deionized water. The following reagents were used in the experiments: NaOH, NaCl, $K_2Cr_2O_7$, $FeCl_3{\cdot}6H_2O$, $(NH_4)_2CO_3$, Diphenylcarbazide, and H_2SO_4. The chromium salt was dissolved in deionized water to prepare a solution with an initial Cr(VI) concentration equal to 20 mg/L, whereas the NaOH and H_2SO_4 solutions were diluted up to 0.1 M and subsequently used to modify the pH of the prepared solutions used for the sorption experiments, measured by a Crison pH-meter.

2.2 Nano-Hematite particles production

The nHP were synthetized according to Xiao et al. (2015). In brief, the $(NH_4)_2CO_3$ was dripped into $FeCl_3{\cdot}6H_2O$ solution by titration device using a molar ratio CO_3^{2-}/Fe(III)=3. The concentration and volume of $FeCl_3{\cdot}6H_2O$ was 1 M and 0.2 L, whereas those of $(NH_4)_2CO_3$ solution added for reaction were 3 M and 0.1 L. At the same time, ethanol was added in order to avoid the aggregation of $Fe(OH)_3$, making the solid–liquid ratio at 1:2. And then the solid phase precipitates were washed alternately with deionized water and alcohol. The crude product would be obtained after filtration with vacuum and dried in the drying oven for 2 hours at 200 °C. The nHP were then characterized by Dynamic Light Scattering (Brookhaven), showing a mean dimension of 46 ± 1.8 nm. Point of Zero Charge (PZC), was determined by suspending different material amounts (0.01, 0.1, 1, 5, 10, 20 % wt) in 0.1 M NaCl solution and measuring the solution pH after 24 h of contact time, according to (Chung et al., 2012). The pH of zero charge measured was equal to 8.3 that was close to the value of 8.2 reported by He et al. (2009) for nHP of 32 nm.

2.3 Experimental set up

The kinetic sorption tests were conducted in a baffled stirred tank reactor, equipped with a Rushton turbine, varying the impeller velocity (8.3, 12.5, 16.6 and 20.8 rps, i.e. 500, 750, 1000 and 1250 rpm). The dimension of the tank diameter, T (m), was 0.123 m, whereas the liquid height, H(m) was fixed equal to T. The impeller diameter, D_i (m) and the clearance, C(m) was fixed equal to 0.33T. The number of baffles was 4 and their dimension was 0.1T. The experiments were conducted at 25°C and pH=3.5, according to preliminary tests where the optimal pH has already been investigated and considering the high pH of zero charge of the material. The initial Cr(VI) concentration was fixed to 20 mg/L whereas the nHP concentration was 6 g/L, according to the Cr(VI)/sorbent concentration used by Xiao et al (2015). The tests were conducted with two identical reactors, and at selected time steps, the same liquid aliquot was withdrawn from the two reactors. The former was used to re-fill the first reactor, to keep its volume constant and to avoid the variation of the hydrodynamic field, whereas the second one was used for the analysis. The nHP were separated through an ultra-centrifuge (14000 rpm for 5 min) and the liquid phase was withdrawn to proceed with the Cr(VI) measure through dyphenyl-carbazide method (Di Palma et al., 2018).

2.4 Data analysis and mathematical modeling

The kinetic sorption data were fitted to the following mass-transfer model:

$$V_T \frac{dCr(VI)}{dt} = -m\frac{dq}{dt} \quad (1)$$

$$\frac{dq}{dt} = \frac{\beta a k_L}{\rho_p}(Cr(VI) - Cr(VI)^{eq}) \quad (2)$$

$$Cr(VI)^{eq} = -\frac{q}{b(q - q_{max})} \quad (3)$$

$$t = 0, \qquad Cr(VI) = Cr(VI)_0 \ and \ q = 0 \quad (4)$$

where V_T (m^3) is the liquid volume in the tank, a (m^2/m^3) is the ratio between liquid film surface onto the particle and the liquid volume in the reactor, m (g) is the sorbent mass, q (mg/g) is the Cr(VI) mass sorbed onto the sorbent material per unit of sorbent mass, β is the sorbent porosity (equal to 0.2 from Adegoke et al (2014), d_p (m) is the sorbent mean size, ρ_p (kg/m^3) is the sorbent particle density (equal to 1.857E+06 g/m^3 from Adegoke et al (2014)), $Cr(VI)^{eq}$ (mg/L) is the equilibrium Cr(VI) concentration according to Langmuir model, b (L/mg) is the Langmuir equilibrium constant (equal to 0.08 L/mg from Adegoke et al (2014)) and q_{max} (mg/g) is the maximum sorption capacity of the sorbent according to Langmuir model (equal to 28.6 mg/g from Adegoke et al (2014)).

The k_L can be correlated to particle Re and Sc number according to Armenante and Kirwan (1989):

$$k_L = \frac{D_{Cr(VI)}}{d_p}\left[2 + 0.52 Re_p{}^{0.52} Sc^{1/3}\right] \quad (5)$$

$$Re_p = \frac{\varepsilon^{1/3} d_p^{4/3}}{\upsilon} \quad (6)$$

$$Sc = \frac{D_{Cr(VI)}}{\upsilon} \quad (7)$$

where $D_{Cr(VI)}$ (m^2/s) is the bulk diffusion coefficient of Cr(VI) species, ν (m^2/s) is the kinematic viscosity of the liquid and ε (W/kg or m^2/s^3) is the local turbulent dissipated energy rate. The model was implemented in gPROMS environment and numerically solved, with k_L and a as model parameters (White and Verdone 2000). The kinetic sorption model equations were coupled with the fluid dynamic model equations through the relation between k_L and ε. The hydrodynamic behavior of a turbulent incompressible fluid (the impeller Reynolds number, $Re=NDi^2/\nu$, was in the range 1.4-3.5 E+04) is governed by the Navier-Stokes equations that can be time-averaged generating the RANS (Reynolds Averaged Navier-Stokes) equations for the velocity **u** (vector) and pressure p (Pa):

$$\frac{\partial \boldsymbol{u}}{\partial t} + \boldsymbol{u} \cdot \nabla \boldsymbol{u} + \nabla p = \nabla \cdot \left((\nu + \nu_T)[\nabla \boldsymbol{u} + \nabla \boldsymbol{u}^T]\right) \quad (8)$$

$$\nabla \cdot \boldsymbol{u} = 0 \quad (9)$$

where ν_T (m^2/s) is the turbulent eddy viscosity which is supposed to emulate the effect of unresolved velocity fluctuations. To close the RANS additional equations and hypotheses are necessary; in particular, the turbulence was modelled using a standard k–ε model for which the transport equations are given by the following PDE (Partial Differential Equation) system:

$$\frac{\partial k}{\partial t} + \nabla \cdot \left(k\boldsymbol{u} - \frac{\nu_T}{\sigma_k}\nabla k\right) + \varepsilon = P_k \quad (10)$$

$$\frac{\partial \varepsilon}{\partial t} + \nabla \cdot \left(\varepsilon \boldsymbol{u} - \frac{\nu_T}{\sigma_\varepsilon}\nabla \varepsilon\right) = \frac{\varepsilon}{k}(C_1 P_k - C_2 \varepsilon) \quad (11)$$

where $\nu_T = C_\mu k^2/\varepsilon$ is the turbulent viscosity, k (J/kg or m^2/s^2) is the turbulent kinetic energy, $P_k = \nu_T/2[\nabla \boldsymbol{u} + \nabla \boldsymbol{u}^T]^2$. The last two terms are responsible for dissipation and production of turbulent kinetic energy, respectively, whereas the default values of the above-reported empirical constants are as follows: C_μ=0.09, C_1=1.44, C_2=1.92, σ_k=1.0, σ_ε=1.3. The system can be solved with proper initial and boundary conditions, already implemented in the software codex (Comsol Multiphysics). The fluid dynamic model was built considering the nHP dispersion in the Cr(VI) solution as a monophasic fluid, since the particle size was small enough to consider this approximation. The mesh (see Figure 1) was composed by 461600 volume elements, 16374 surface elements and 1164 boundary elements; Impeller region (less than 2% of tank volume) was meshed with more than 10% of the total grid size used for the full tank in order to resolve the steep gradients in the impeller region (as well as the regions near vessel wall and baffle were more densely meshed).

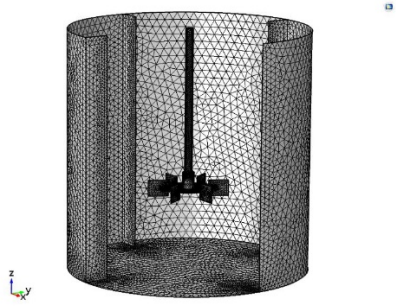

Figure 1: mesh built in Comsol software.

The predicted ε values were used to estimate the k_L variation in the agitated liquid volume. The maximum predicted ε value was also compared with that calculated according to the following correlation (Mc Cabe et al., 1993):

$$\varepsilon_{cal} = 20\varepsilon_g = 20\frac{P}{V_T \rho_L} = 20\frac{N_P N^3 D_i^5}{V_T} \quad (12)$$

where P (W) is the power required to drive the impeller, ε_g ($m^2\ s^{-3}$) is the turbulent kinetic energy dissipation rate referred to the tank (usually one or two order of magnitude lower in comparison to the value observed close to the impeller), N (rps) is the impeller velocity and N_p is the impeller power number (for a Rushton impeller and for Re>2000 N_p is constant and equal to 5 (Mc Cabe et al., 1993)).

3. Results and Discussion

3.1 Influence of impeller rotational velocity on Cr(VI) removal

Figure 2 displays the obtained kinetic data at different N values.

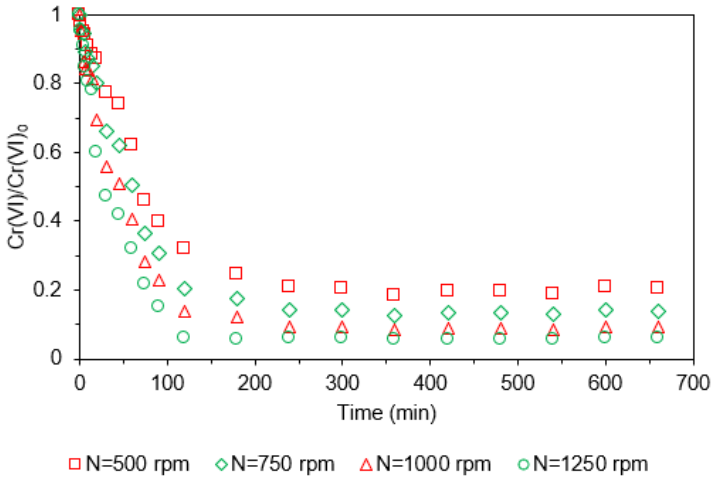

Figure 2: Cr(VI) equilibrium data over time at different impeller velocity (temperature=25°C, $Cr(VI)_0$=20 mg/L, nHP concentration=6 g/L).

It can be clearly observed from the above reported graphs that an increase in the impeller velocity led to an increase of the final Cr(VI) removal efficiency, without varying the trends. More in detail, the Cr(VI) removal efficiency values were 79.5, 86, 90.8 and 94% for N=500, 750, 1000 and 1250 rpm, respectively. Another important result was that the asymptote of Cr(VI) concentration was reached before 300 min when the N value was increased from 500 up to 1000 rpm, since the asymptotic Cr(VI) concentration value was reached after 180 min. Similar results have been reported by other authors, where Cr(VI) removal up to 85% have been reached using 3 g/L of nHP in acid environment (Liu et al., 2010).
Through Eqs. (5), (6), (7) and (12) a first evaluation of the N influence on the mass transfer process efficiency was performed, as reported in figure 3.

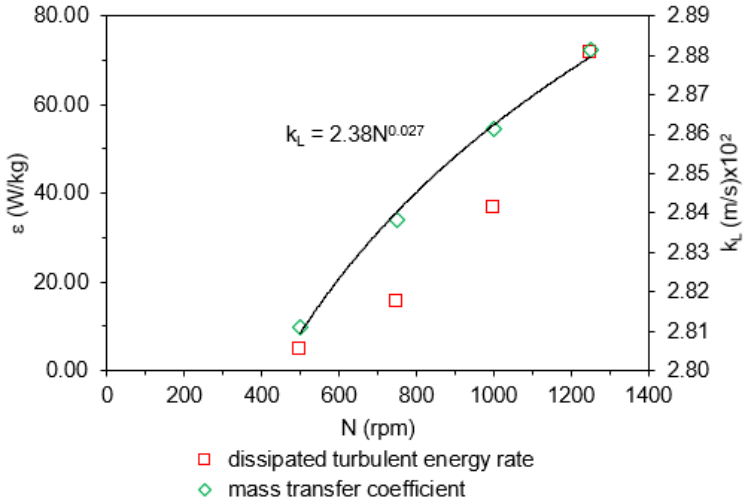

Figure 3: ε and k_L values obtained from empirical correlations.

As expected, the ε and k_L increased with N increase. However, the k_L increase was quite restrained (about 3% from N=500 up to N=1250 rpm) in comparison with the Cr(VI) removal efficiency enhancement (from 79.5 to 94%) implying that the hydrodynamic conditions variation influence on the process should be quantified with more suitable parameters. For instance, the turbulent dissipated energy rate increase, better justified the overall process efficiency improvement, since it increased from 4.6 up to 71.7 W/kg, passing from N=500 up to N=1250 rpm. Indeed, it is well known that larger e values led to higher mixing efficiency, therefore to higher mass transfer rate in agitated liquid/solid systems (Paul et al., 2004). From the CFD simulations the

distribution of both ε and k_L in the tank liquid volume for N=500 and N=1250 rpm was obtained and reported in Figure 4.

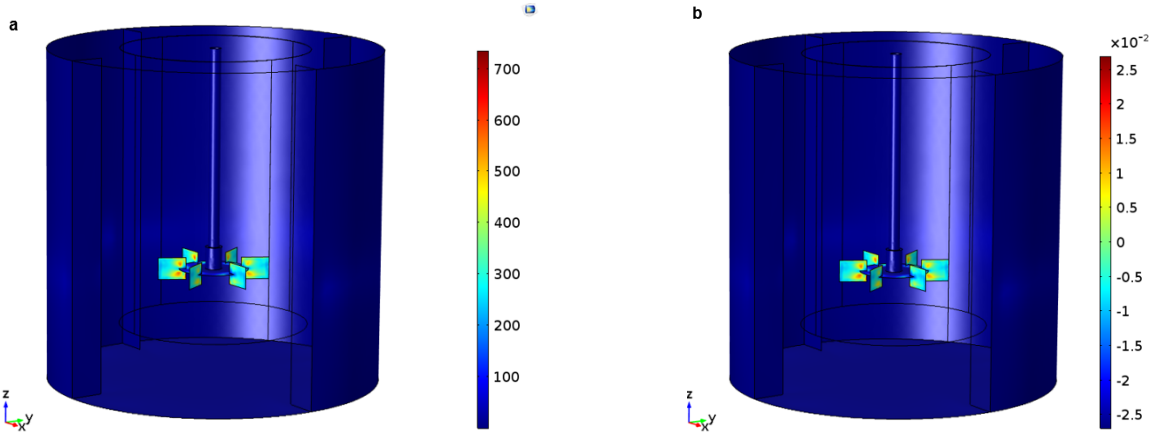

Figure 4: ε and k_L values for N=1250 rpm (a,b).

The mass transfer coefficient values predicted from the model were in agreement with those estimated by empirical correlations. Indeed, the CFD model calculated a distribution of both ε and k_L values, where the maximum k_L value on the impeller tips (2.61 m/s x 10^{-2}), was very close to the 2.88 x 10^{-2} m/s previously calculated.

3.2 Kinetic data modelling

Figure 5 shows the kinetic mass transfer model fitted on the experimental data and the relation between regressed k_L and N.

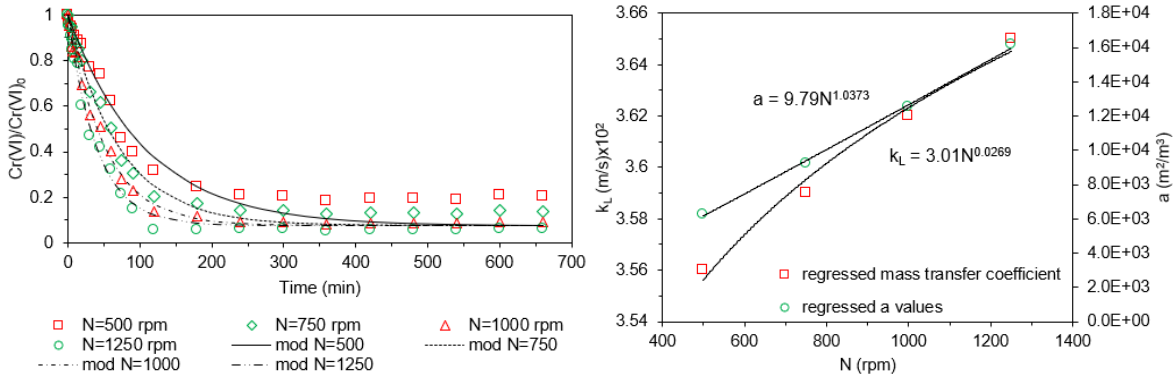

Figure 5: results of mass-transfer model fitting on experimental data (a) and regression k_L relation with impeller velocity (b).

The model was able to describe the overall experimental data trend, particularly for higher impeller velocity, since the R^2 coefficient increased from 0.9 to 0.99 when the impeller velocity passed from 500 up to 1250 rpm. Regarding the regressed k_L values, their order of magnitude was the same of those calculated through Eq. (5) and the regressed power law was characterized by the same order for N and similar coefficient. Another important result was the quasi-linear trend between regressed a values and N, that was in line with the expectations.

4. Conclusions

Hematite nanoparticles were synthetized by lab-scale equipment, showing a mean size of 46 nm and unimodal distribution. The nanoparticles were employed in a Rushton equipped stirred tank reactor to remove Cr(VI) in synthetic wastewaters. The results at increasing impeller velocity values showed the suitability of this nanomaterial towards Cr(VI) removal by sorption mechanism. In detail, the variation of impeller velocity in the range 500-1250 rpm, at fixed geometry, pH=3.5, Cr(VI)=20 mg/L and nHP=6 g/L, led to 79.5, 86, 90.8 and

94% of Cr(VI) removal efficiencies. The kinetic experiments showed that the Cr(VI) removal asymptotic value was reached at 300 min for N=500 and 750 rpm, whereas decreased to 240 min for N=100 rpm and to 120 min for N=1250 rpm. The employed mass-transfer model was able to describe the overall phenomenon and the regressed k_L values were in agreement with those obtained by CFD simulations and by empirical correlations.

References

Acar F. N., Malkoc E., 2004, The removal of chromium (VI) from aqueous solutions by Fagus orientalis L, Bioresource technology, 94(1), 13-15.

Adegoke H. I., AmooAdekola F., Fatoki O. S., Ximba B. J., 2014, Adsorption of Cr (VI) on synthetic hematite nanoparticles of different morphologies, Korean Journal of Chemical Engineering, 31(1), 142-154.

Armenante P. M., Kirwan D. J., 1989, Mass transfer to microparticles in agitated systems, Chemical Engineering Science, 44(12), 2781-2796.

Bavasso I., Montanaro D., Petrucci E., Di Palma L., 2017, Shortcut biological nitrogen removal (sbnr) in microbial fuel cells (mfcs), Chemical Engineering Transactions, 57, 727-732.

Bavasso I., Montanaro D., Petrucci E., Di Palma L., 2018a, Shortcut Biological Nitrogen Removal (SBNR) in an MFC Anode Chamber under Microaerobic Conditions: The Effect of C/N Ratio and Kinetic Study, Sustainability, 10(4), 1062.

Bavasso I., Verdone N., Di Palma L., 2018b, Cr(VI) Removal by Green-Synthetized Iron-Based Nanoparticles: Effect of Cr(VI) Concentration and pH Condition on Adsorption Process, Chemical Engineering Transactions, 70, 469-474.

Chen Y. H., Liu D. Y., Lee J. F., 2018, Study of Cr (VI) adsorption onto magnetite nanoparticles using synchrotron-based X-ray absorption spectroscopy, Physics and Chemistry of Minerals, 45, 907-913.

Di Pascasio F., Genova V., Gozzi D., Latini A., Lazzarini L., 2016, High temperatures gas-solid reactivity of aluminum-carbon nanotubes composites, Thermochimica Acta, 640, 8-18.

Di Palma L., Verdone N., Vilardi G., 2018, Kinetic Modeling of Cr(VI) Reduction by nZVI in Soil: The Influence of Organic Matter and Manganese Oxide, Bulletin of Environmental Contamination and Toxicology, 101, 692-697.

Genova V., Marini D., Valente M., Marra F., Pulci G., 2017, Nanostructured Nickel Film Deposition on Carbon Fibers for Improving Reinforcement-matrix Interface in Metal Matrix Composites, Chemical Engineering Transactions, 60, 73-78.

He Y. T., Wan J., Tokunaga T., 2008, Kinetic stability of hematite nanoparticles: the effect of particle sizes, Journal of nanoparticle research, 10, 321-332.

Konuray A. O., Liendo F., Fernández-Francos X., Serra À., Sangermano M., Ramis X., 2017, Sequential curing of thiol-acetoacetate-acrylate thermosets by latent Michael addition reactions, Polymer, 113, 193-199.

Liu T. Y., Zhao L., Tan X., Liu S. J., Li J. J., Qi Y., Mao G. Z., 2010, Effects of physicochemical factors on Cr (VI) removal from leachate by zero-valent iron and α-Fe2O3 nanoparticles, Water Science and Technology, 61(11), 2759-2767.

Mc Cabe W.L., Smith J.C., Harriott P., Unit Operations of Chemical Engineering, McGraw-Hill, 1993.

Paul E. L., Atiemo-Obeng V. A., Kresta S. M., 2004, Handbook of industrial mixing: science and practice, John Wiley & Sons.

Patterer M. S., Bavasso I., Sambeth J. E., Medici F., 2017, Cadmium removal from acqueous solution by adsorption on spent coffee grounds, Chemical Engineering Transactions, 60, 157-162.

Scargiali F., Busciglio A., Grisafi F., Brucato A., 2014, Mass transfer and hydrodynamic characteristics of unbaffled stirred bio-reactors: influence of impeller design, Biochemical engineering journal, 82, 41-47.

Singh D. B., Gupta G. S., Prasad G., Rupainwar D. C., 1993, The Use of Hematite for Chromium(VI) Removal, Journal of Environmental Science and Health. Part A: Environmental Science and Engineering and Toxicology, 28, 1813-1826.

Stoller M., Di Palma L., Vuppala S., Verdone N., Vilardi G., 2018, Process intensification techniques for the production of nano-and submicronic particles for food and medical applications, Current Pharmaceutical Design, 24, 2329-2338.

White D. A., Verdone N., 2000, Numerical modelling of sedimentation processes, Chemical Engineering Science, 55, 2213-2222.

Xiao Q., Sun Y., Zhang J., Li Q., 2015, Size-dependent of chromium (VI) adsorption on nano α-Fe2O3 surface, Applied Surface Science, 356, 18-23.